cosmetics

MDPI

*Article*

# HA20, a Broad-Molecular-Weight Hyaluronic Acid Complex, Supports Transepidermal Bioavailability and Multi-Stress Barrier Protection in Human Skin Models

**Zheng Wang [1,*], Yumei Fan [1], Luxian Zhou [2], Dandan Jiang [2], Jiajun Qian [1] and Peixue Ling [3,*]**

[1] Meyer Bio-Medicine Co., Ltd., Jinan 250022, China; bzguo9@163.com (Y.F.)
[2] Shanghai Archgene Biotechnology Co., Ltd., Shanghai 200233, China
[3] National Glycoengineering Research Center, Qingdao Campus, Shandong University, Qingdao 266237, China
* Correspondence: wz252994727@126.com (Z.W.); lingpeixue@126.com (P.L.)

## Abstract

Hyaluronic acid (HA) is widely used in skincare, but its efficacy varies with molecular weight (MW), affecting its skin penetration and activity. This study examined whether HA20, a broad-MW HA complex (weight-average MW: 188 kDa, 10–1000 kDa), improves skin absorption and shields human skin models from environmental stress. HA transepidermal bioavailability, extracellular-matrix responses, glyoxal-induced Nε-(carboxymethyl)lysine (CML), UVA-induced mitochondrial membrane potential (MMP) loss, Th2 cytokine-induced markers, and dryness-induced barrier changes were assessed in reconstructed human epidermis, dermal fibroblasts, and epidermal keratinocytes. HA20 exhibited greater apparent permeation detectable by ELISA at all time points during the 24 h RHE assay compared to high-MW HA. In fibroblasts, 0.05% HA20 increased type I collagen secretion from 535.20 to 585.47 pg/mL and elastin from 8.68 to 9.24 pg/mL, reduced CML fluorescence to 70.13% of the glyoxal control, and increased MMP-associated fluorescence from 58.76% in the UVA model group to 298.86%. In keratinocytes, 0.1% HA20 reduced IL-4/IL-13-induced *NELL2* and *CAII* expression. Under acute dryness, HA20 maintained stratum corneum morphology and altered transcriptomic signatures related to epidermal differentiation, extracellular matrix organization, and barrier-associated genes, including *KRT37*, *COL7A1*, *ACER2*, and *SPRR1A*. These findings suggest that HA20 supports barrier resilience mainly through improved transepidermal delivery and ECM or barrier-repair responses.

**Keywords:** Hyaluronic acid; molecular weight distribution; skin exposome; anti-glycation; transcriptomics; cutaneous dryness

Check for updates

Academic Editor: Enzo Berardesca

Received: 19 May 2026
Revised: 30 June 2026
Accepted: 10 July 2026
Published: 13 July 2026

**Copyright:** © 2026 by the authors. Licensee MDPI, Basel, Switzerland. This article is an open access article distributed under the terms and conditions of the Creative Commons Attribution (CC BY) license.

## 1. Introduction

Hyaluronic acid (HA) is a non-sulfated glycosaminoglycan that is abundantly present in the extracellular matrix (ECM) of human skin. It has been known for its excellent hygroscopic properties and biocompatibility in dermatology and cosmetology [1]. The skin levels of HA are around 50% of the body's total HA [2], and they play an important role in hydration, elasticity and firmness of the skin [3,4]. But age causes a natural degradation in HA production, which can cause less water binding, dry skin and formation of wrinkles [4]. These aging phenotypes are mitigated with topical HA treatment and its ability to maintain skin health [3].

The biological functions and physicochemical properties of HA are not fixed but vary significantly with molecular weight (MW) [5]. This MW dependence is a key mechanism by which HA influences physiological balance, pathological changes, and various biomedical or dermatological uses. Generally, high-MW HA (>1000 kDa) and very-high-MW HA (>6000 kDa) are mainly involved in surface hydration, viscoelasticity, organizing the ECM, and supporting the skin barrier. In contrast, medium- and low-MW HA fractions tend to be more accessible within tissues and can interact more easily with HA-binding receptors such as CD44, RHAMM, TLR2/4, ICAM-1, and Layilin [5,6]. This MW-dependent behavior creates a biological "MW paradox," in which HA bioactivity shows a nonlinear, sometimes opposing, relationship with molecular size: high-MW HA is generally associated with anti-inflammatory, immunomodulatory, and tissue-homeostatic effects, whereas Low-MW HA or oligomeric fragments often promote pro-inflammatory signaling, angiogenesis, and cell proliferation [5–7]. Consistent with this MW-dependent size–function relationship, Raman spectroscopy studies have shown that high-MW HA (1000–1400 kDa) is mainly retained within the superficial stratum corneum (SC), reaching a penetration depth of approximately 25 μm, whereas intermediate-MW HA (100–300 kDa) and low-MW HA (20–50 kDa) penetrate more deeply, reaching approximately 50 and 100 μm, respectively [8]. But the relationship between penetration and activity is complex, and the low MW HA can penetrate deeper layers and can show high biological activity [9]. It has also been reported to increase transepidermal water loss [10], suggesting that there may be a problem with barrier integrity. Beyond physical penetration, the molecular size of HA determines its bioactivity. Recent evidence indicated that both low and high MW HA upregulated important tight junction proteins such as the claudins 3 and 4, while high MW HA had a larger effect, also inducing the expression of the junctional adhesion molecule 1 [11]. HA oligosaccharides of 2 kDa were found to rejuvenate the deep dermis by regulating collagen metabolism, which helps counteract skin sagging [12]. Furthermore, HA with a MW in the transition range (approximately 200 kDa) is the unique signaling node that can trigger the trimerization of stabilin-2 and thereby initiate pro-survival signaling through the NF-κB and ERK pathways [7]. These findings indicate that an optimized, broad-spectrum MW distribution is necessary to balance surface barrier reinforcement with deep-seated signaling.

As the largest organ in the human body, the skin is continuously exposed to the skin exposome, which includes a diverse range of exogenous and endogenous stressors such as ultraviolet (UV) radiation, environmental factors, and metabolic byproducts [13]. UV radiation is a major component of this exposome and contributes to premature cutaneous aging, manifesting as wrinkles, hyperpigmentation, and loss of elasticity [14]. Glycation causes the accumulation of advanced glycation end-products (AGEs), particularly Nε-(carboxymethyl)lysine (CML) [15]. CML accumulation irreversibly cross-links and stiffens the collagen-elastin network. This extensive ECM degradation causes dermal loss of elasticity, and triggers a cascade of structural remodeling, which fundamentally driving the formation of aged skin [16].

Moreover, the epidermal compartment faces unique exposome challenges, notably immune-mediated neurogenic sensitization and severe environmental dryness [17,18]. In conditions like atopic dermatitis (AD) and hyper-reactive skin syndrome, the Th2-mediated inflammatory microenvironment, is mainly driven by interleukin (IL)-4 and IL-13. This environment compromises the epidermal barrier, and orchestrates neuro-epidermal crosstalk. In this process, keratinocytes aberrantly express neurogenic and pruritus-associated markers, which contribute to the debilitating itch-scratch cycle [19–21]. Despite the demonstrated potential of HA in hydration and certain biological functions, studies on its efficacy in addressing the complex and dynamic stressors of the skin exposome

remain relatively limited. Although recent academic reviews suggest that HA has the potential to reduce glycation-induced stress [22], but there is a lack of empirical evidence regarding the direct interception capability of topically applied HA to CML accumulation. Moreover, while the moisturizing effect of HA is well-documented, the specific genomic regulatory mechanisms by which HA contributes to barrier protection, especially under extreme dryness conditions, are largely unexplored. Therefore, this study evaluated the multi-targeted exposome defense potential of HA20, which is an optimized broad-spectrum MW HA (weight-average MW (Mw): Approximately 200 kDa; range: 10–1000 kDa).

Based on the MW-dependent physical and biological framework described above, we hypothesize that HA20 utilizes its polydispersity to achieve layered skin penetration. In this model, the low MW fractions penetrate into the deep dermis to repair UVA-induced damage, whereas the intermediate-MW fractions remain in the viable epidermis to trigger a structural repair program. This study uses primary human cells and a 3D reconstructed human epidermis (RHE) model to investigate the capacity of HA20 to stimulate ECM remodeling, reduce glyoxal-induced glycation, dampen neurogenic pruritus signaling, and strengthen the skin barrier under extreme dryness stress.

## 2. Materials and Methods

### 2.1. Reagents and Chemicals

High-MW HA (1300–1500 kDa) was provided by Shandong Guantianxia Biotechnology Co., Ltd. (Linyi, China). The Cell Counting Kit-8 (CCK-8) was acquired from Dojindo Laboratories (Kumamoto, Japan). For ECM quantification, the Human Collagen Type I ELISA Kit was purchased from Bioswamp Technology (Wuhan, China), and the Human Elastin ELISA Kit was obtained from Cusabio Technology (Wuhan, China). The highly specific Hyaluronan Quantikine ELISA Kit and recombinant human IL-4 and IL-13 were provided by R&D Systems (Minneapolis, MN, USA). Glyoxal and the glycation inhibitor aminoguanidine (AG) were acquired from Sigma-Aldrich (St. Louis, MO, USA). For immunofluorescence, the primary antibody against CML was acquired from Abcam (Cambridge, UK). A mitochondrial membrane potential (MMP) detection kit for live cells, using the Mito-Tracker Deep Red 633 probe, was supplied by Beyotime Biotechnology (Shanghai, China).

### 2.2. Preparation and MW Characterization of HA20

HA20 was prepared by a patented multi-stage degradation and blending process [23] with minor laboratory adjustments. Briefly, high-MW HA (1000 kDa) was exposed to UV irradiation for 60 min to begin the primary chain scission. The irradiated HA was dissolved in deionized water to make a 1% ($w/v$) solution. Then, this solution was subjected to ultrasonic treatment at a 10 kHz frequency for 15 min. This was done to further tailor the MW distribution. To create the full-spectrum profile, we blended the degraded solution with a 1% ($w/v$) solution of native HA (100 kDa) at a specific mass ratio. The mixture was purified by adding 0.1% ($w/v$) diatomaceous earth and 0.1% ($w/v$) activated carbon for adsorption and decolorization, respectively. The resulting solution was then concentrated and further purified by nanofiltration using a membrane with an MW cut-off of 200–300 Da to remove residual salts and low-MW degradation byproducts. The purified concentrate was spray-dried, and the HA20 powder was stored in a desiccator at room temperature.

The final HA20 material underwent standard quality control tests. Endotoxin levels were measured using the gel-clot LAL method in accordance with Chinese Pharmacopoeia General Rule 1143 (2020) [24], while protein content was assessed with the Coomassie Brilliant Blue assay. Results showed an endotoxin level of <0.01 EU, protein content of <0.01%, and absorbance values at 260 and 280 nm both below 0.01.

MW and the polydispersity of HA20 were determined via gel permeation chromatography (GPC) with an Agilent 1260 Infinity II system equipped with a Refractive Index Detector (Agilent Technologies, Santa Clara, CA, USA). The separation was done by connecting two columns in series: Waters Ultrahydrogel 1000 and Waters Ultrahydrogel 120 (Waters Corporation, Milford, MA, USA). The mobile phase was a 0.1 M $NaNO_3$ aqueous solution, kept at a 0.8 mL/min flow rate, and the column temperature was 40 °C. Polyethylene oxide standards with various MWs were used to establish the calibration curve. The samples were dissolved in the mobile phase, and the injection volume was 100 µL.

### 2.3. Cell Culture

Normal Human Dermal Fibroblasts (NHDFs) and Normal Human Epidermal Keratinocytes (NHEKs) were obtained from Lifeline® Cell Technology (Frederick, MD, USA). To maintain optimal primary cell phenotypes, NHDFs were cultured in FibroLife® serum-free medium supplemented with the associated LifeFactors® kit (LifeFactors Lifeline Cell Technology, Frederick, MD, USA), while NHEKs were maintained in DermaLife® K serum-free medium, following the manufacturer's instructions. All cell cultures were incubated in a standard humidified atmosphere at 37 °C with 5% $CO_2$.

### 2.4. In Vitro Skin Permeation Kinetics in a 3D-RHE Model

To simulate the physiological complexity of the human skin barrier, an RHE model (ArchSkin®, Archgene Biotechnology, Shanghai, China) was used as the permeation membrane for the transepidermal assay. Using 3D-RHE tissues as a predictive surrogate for human skin penetration is adapted from validated methodologies [25,26], demonstrating that mature RHE tissues possess stratified SC and lipid lamellae analogous to in vivo human skin. Briefly, RHE models were cultured at the air-liquid interface for 12 days in a chemically defined, serum-free medium to facilitate a fully stratified epidermis formation consisting of a basal layer, spinous layer, granular layer, and a functional SC. Aqueous formulations containing 0.1% HA20 or high-MW HA were topically applied to the apical surface of RHE tissues. For each RHE insert, exactly 10 µL of each HA formulation was placed at the center of the SC surface. Immediately after pipetting, the droplet was gently spread across the entire epidermal surface using a sterilized, fire-polished glass rod with a smooth, rounded bulb-shaped tip. The glass rod was moved in light circular motions to ensure the surface was evenly and thoroughly wetted without causing mechanical abrasion, scratching, or disrupting the SC. To profile penetration kinetics, receiver fluids from the basolateral compartment were collected at predefined time intervals of 0, 4, 8, 12, and 24 h. The cumulative amount of penetrated HA at each time point was quantitatively determined using the highly specific Hyaluronan Quantikine ELISA Kit. The manufacturer states that this kit measures HA $\geq$ 35 kDa. As a result, the ELISA outcomes reflect the detectable apparent HA permeation and not the total HA20 permeation, especially for fractions under 35 kDa. A preliminary in vivo Raman spectroscopy comparison of HA20 and high-MW HA is detailed in Figure S1 and Tables S1 and S2.

### 2.5. Assessment of Cell Viability and ECM Synthesis in NHDFs

NHDF cell viability following HA20 treatment was determined using the CCK-8 assay. For ECM analysis, NHDFs were treated with various HA20 concentrations for 48 h. Type I collagen and elastin secretion into the culture supernatant was quantified using commercially available ELISA kits, following the manufacturer's instructions.

### 2.6. Evaluation of Anti-Glycation Efficacy and CML Accumulation in NHDFs

To assess the anti-glycation efficacy, we set up an AGE model in NHDFs using glyoxal, as outlined in prior work [15]. Briefly, NHDFs were plated into 12-well plates and cultured

until reaching around 70% confluence. For glycation induction and CML accumulation, cells were treated with 0.5 mM glyoxal over 48 h. After this phase, the medium was replaced, and cells were co-treated with 0.05 mM glyoxal plus specified doses of HA20 (or AG as a positive control) for an additional 48 h. In immunofluorescence staining, treated cells were washed with phosphate-buffered saline and fixed with 4% paraformaldehyde overnight at 4 °C. Fixed cells were then permeabilized using 0.1% Triton X-100 for 5 min at room temperature. The fixed cells were permeabilized with 0.1% Triton X-100 solution for 5 min at room temperature. Non-specific binding sites were blocked by incubating the cells with 1% bovine serum albumin for 1 h. Next, cells were incubated with a primary anti-CML antibody (1:50 dilution) overnight at 4 °C. After two phosphate-buffered saline washes, a donkey anti-mouse Alexa Fluor® 488-conjugated secondary antibody (1:1000 dilution) was applied for 2 h at room temperature in the dark. Nuclei were counterstained, and slides were mounted with an anti-fade medium containing DAPI. Fluorescence images were captured via a Leica fluorescence microscope (Wetzlar, Germany). Finally, the relative fluorescence intensity of CML was measured using ImageJ software, version 1.53e (NIH, Bethesda, MD, USA) from randomly selected visual fields in each group.

The nuclei were counterstained, and the slides were mounted using an anti-fade mounting medium containing DAPI. Fluorescence images were captured using a fluorescence microscope (Leica, Wetzlar, Germany). The relative fluorescence intensity of CML was quantified using the ImageJ software from randomly visual fields per group.

### 2.7. Protective Effects Against UVA-Induced Photo-Oxidative Stress

NHDFs were first pre-treated overnight with a specified concentrations of HA20, then exposed to UVA irradiation (10 J/cm$^2$) to trigger photo-oxidative stress. The MMP ($\Delta\Psi$m) was assessed using a membrane potential-dependent fluorescent probe, strictly following the manufacturer's instructions for MMP measurement. HA20's protective efficacy was quantified by measuring the retained deep red fluorescence, which directly indicates the preservation of mitochondrial polarization.

### 2.8. Anti-Inflammatory Evaluation in a Th2-Induced AD Cell Model

To mimic a Th2-induced inflammatory microenvironment typical of AD and sensitive skin, we seeded NHEKs in 6-well plates and cultured them to 70–80% confluence. Then, the cells were stimulated with a recombinant cytokine cocktail, which contains IL-4 and IL-13, each at 10 ng/mL. The cells were exposed to a specified concentration of HA20, and were incubated for a duration of 72 h. After the treatment, total RNA was extracted from NHEKs with the RNeasy Mini Kit (QIAGEN, Hilden, Germany)) and then reversed-transcribed to cDNA. Quantitative real-time polymerase chain reaction (PCR) was carried out with SYBR Green Master Mix (ABclonal, Wuhan, China) on a QuantStudio 7 Flex system. The relative mRNA expression levels were determined by the $2^{-\triangle\triangle CT}$ method. The primer sequences used in this study are provided in Table 1.

**Table 1.** The sequences of primers used for PCR.

| Target Gene | Primer Sequences (5′ to 3′) | |
|---|---|---|
| | Forward | Reverse |
| *CAII* | AACAATGGTCATGCTTTCAACG | TGTCCATCAAGTGAACCCCAG |
| *NELL2* | TAAGGGTATAATGCAAGATGTCCAATT | AGATCTGGGCACTGAGCAATAAA |
| *FLG* | TGAAGCCTATGACACCACTGA | TCCCCTACGCTTTCTTGTCCT |
| *LOR* | GTCTGCGGAGGTGGTTCCTCT | TGCTGGGTCTGGTGGCAGATC |
| *KRT37* | ACCACCAGGATGTGGAACAGTG | CATTCACCGTGCATCTCAGCTC |
| *COL7A1* | GTTGGAGAGAAAGGTGACGAGG | TGGTCTCCCTTTTCACCCACAG |

**Table 1.** *Cont.*

| Target Gene | Primer Sequences (5′ to 3′) | |
|---|---|---|
| | Forward | Reverse |
| *ACER2* | CCTGTTCTGCTGGATCAGTGAC | GTAGGCAAAGCATACACAGCCC |
| *SPRR1A* | GTGAAACAACCTTGCCAGCCTC | TGGCAGGGCTCTGGAACCTTG |
| *YWHAZ* | ACCGTTACTTGGCTGAGGTTGC | CCCAGTCTGATAGGATGTGTTGG |

### 2.9. Barrier Repair and Histological Evaluation Under Dryness Stress in 3D-RHE

To evaluate how well HA20 protects and repairs tissues under severe dryness, we applied a standardized physical dryness model, which is adapted from the protocol by Viodé et al. [27]. In short, we precisely controlled relative humidity (RH) to mimic extreme dryness, which allowed us to evaluate both structural integrity and transcriptomic changes under stress. Before triggering dryness, the apical side of tissues in the treatment group received a topical pre-treatment with 0.1% HA20. These tissues were then exposed to acute dryness (below 20% RH) for a period of 2 h. Immediately following this stress phase, a second topical application of 0.1% HA20 was administered. All tissues were then returned to a standard incubator (37 °C, 5% $CO_2$) for a 24 h recovery period. For histological analysis, harvested RHE samples were bisected, fixed in 4% paraformaldehyde, dehydrated, embedded in paraffin, and sectioned at 5 µm thickness. Standard hematoxylin and eosin (H&E) staining was performed to assess general epidermal architecture and the structural integrity of the SC.

### 2.10. Transcriptomic Profiling and qPCR Validation in 3D RHE

To preserve RNA integrity for subsequent transcriptomic analysis, the remaining halves of the harvested RHE tissues were immediately snap-frozen in liquid nitrogen. Following this, total RNA was extracted using TRIzol™ Reagent. The quality of the isolated RNA was then rigorously assessed with an Agilent 2100 Bioanalyzer (Agilent Technologies, Santa Clara, CA, USA). We prepared the sequencing libraries using the NGS® Ultima Dual-mode mRNA Library Prep Kit from Yeasen Biotechnology (Shanghai, China), following the manufacturer's protocol. The libraries were then sequenced on an Illumina NovaSeq X Plus platform (San Diego, CA, USA). For data analysis, we used the DESeq2 package to identify differentially expressed genes (DEGs). We focused on pathways related to epidermal structure and lipid metabolism. Genes were considered significantly changed if they had an adjusted $p < 0.05$ and $|\log_2 FC| > 1.2$. To confirm the sequencing results, we performed quantitative PCR after RNA extraction and cDNA synthesis, as described in Section 2.8. All primer sequences used for quantitative PCR are listed in Table 1.

### 2.11. Statistical Analysis

Data are presented as mean ± standard deviation (SD). Statistical analyses were done using R software (version 4.4.2). To compare multiple groups, we used one-way analysis of variance, followed by Tukey's post hoc test to check for differences between groups. All statistical tests were two-tailed, and results with $p < 0.05$ were considered statistically significant.

## 3. Results

### 3.1. MW Distribution of HA20

GPC analysis was performed to confirm MW and distribution of the prepared HA20. As shown in Figure 1, weight-average MW ($M_W$) of HA20 was approximately 188 kDa, measured at 188,091 Da, while the number-average MW (Mn) was 92,735 Da. The peak

MW (Mp) was 178,464 Da. The polydispersity index (Mw/Mn) was 2.03, indicating a broad molecular weight distribution consistent with the multi-stage degradation and blending processes described in the Methods section. A detailed analysis of the distribution shows a balanced, full-spectrum profile. The HA20 complex had four equal fractions, each making up 25% of the total, spread across molecular weight ranges of less than 88.2 kDa, 88.2 to 155.1 kDa, 155.1 to 252.4 kDa, and more than 252.4 kDa. This profile shows that HA20 is not a single-size fraction but a purposely designed complex centered at 200 kDa, made to include a wide range of biologically active fragments.

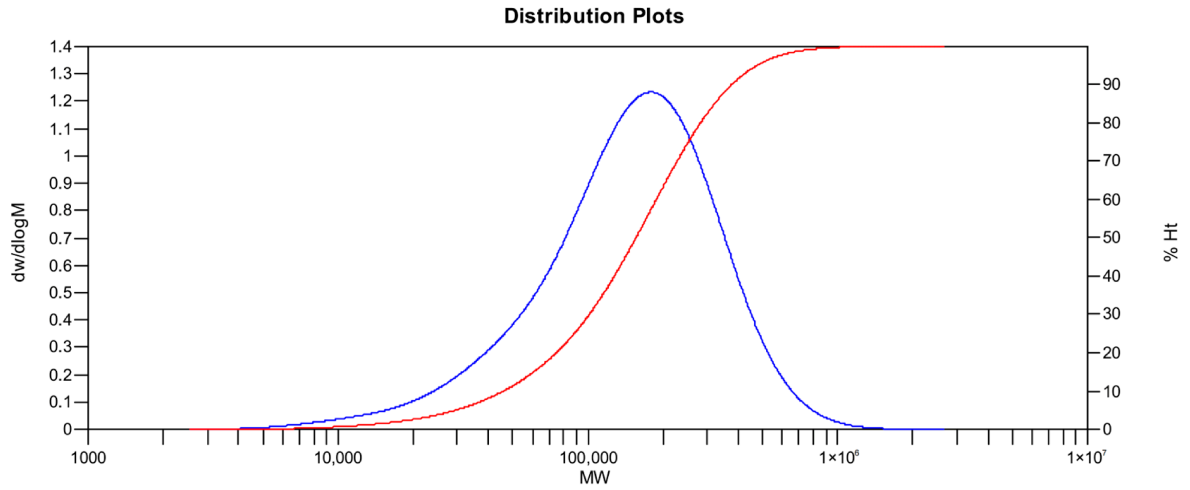



**Figure 1.** Molecular weight distribution of HA20 determined by GPC analysis. The blue line shows the differential MW distribution curve, labeled dw/dlogM, which illustrates how HA molecules are distributed across various MW ranges. The red line depicts the cumulative MW distribution curve, represented as %Ht, indicating the total mass fraction of HA molecules below a specific MW.

### *3.2. HA20 Showed Greater Apparent Transepidermal Bioavailability than High-MW HA in 3D RHE Models*

The apparent transepidermal permeation of HA20 and high-MW HA, detectable by ELISA, was assessed over a 24 h period (Figure 2). In both groups, the total permeation increased over time, with HA20 showing higher apparent permeation than high-MW HA. HA20 exhibited a rapid initial permeation rate, reaching 23.8% at 4 h compared to 14.8% for high-MW HA. By 24 h, HA20 achieved an apparent cumulative permeation of 31.1%, while high-MW HA reached 22.4%. These findings suggest that the ELISA-detectable portion of HA20 demonstrated greater apparent transepidermal transport than high-MW HA. However, since HA20 contains low-MW fractions below the ELISA detection limit, the assay likely underestimates the total HA20 penetration. A small in vivo Raman spectroscopy study ($n$ = 3), shown in Figure S1 and Tables S1 and S2, indicated higher relative penetration for HA20 than high-MW HA at 2, 4, 8, and 10 h, supporting the trend observed in the RHE model but should be interpreted with caution due to the limited sample size.

### *3.3. HA20 Stimulated the Collagen I and Elastin Secretion in NHDFs*

The biocompatibility and biological effects of HA20 were tested on NHDFs. As shown in Figure 3A, HA20 had non-significant cytoxicity across a wide concentration range (0.0001% to 0.1%), with cell viability staying close to 100%. This shows that HA20 has a very good biocompatibility.

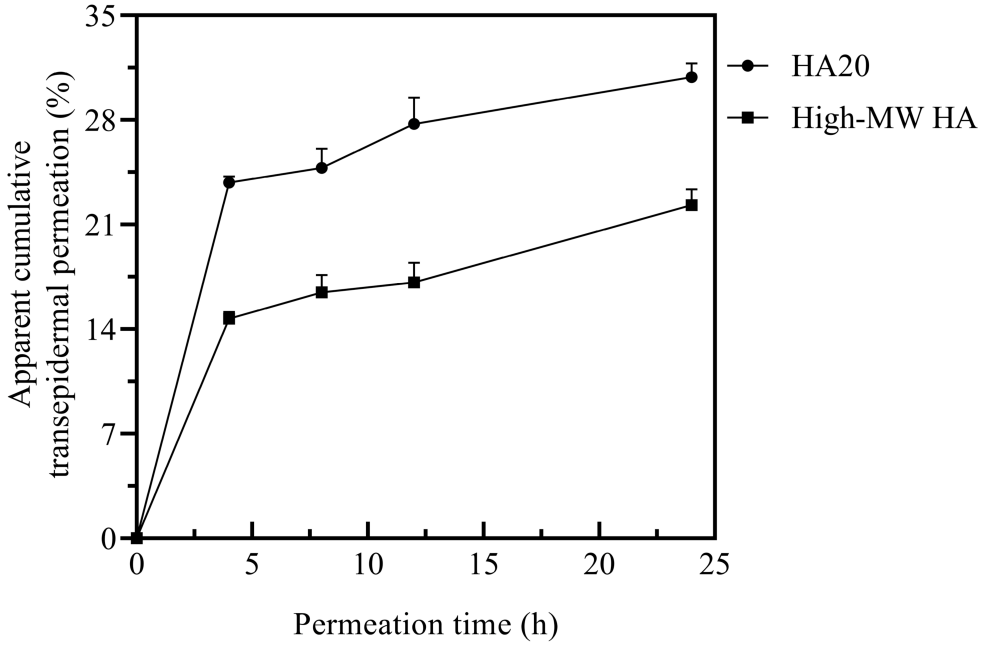



**Figure 2.** ELISA-detectable apparent transepidermal permeation rates of HA20 and high-MW HA over 24 h. The Hyaluronan Quantikine ELISA Kit detects HA fractions of 35 kDa or higher, so these values reflect ELISA-detectable apparent permeation, not total HA permeation. Since HA20 includes fractions smaller than 35 kDa, its total permeation might be underestimated.

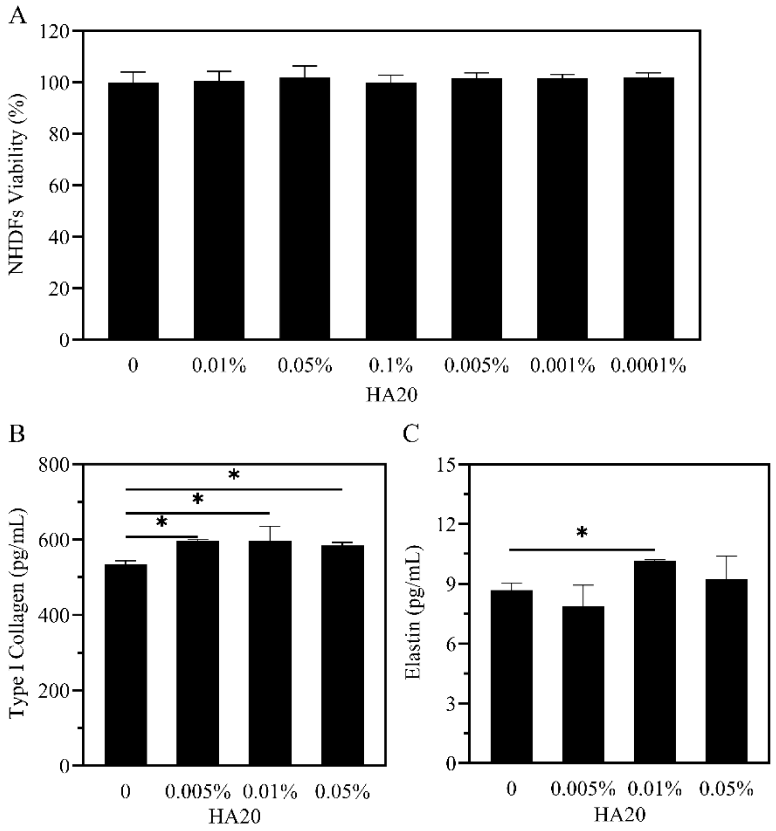



**Figure 3.** Effect of HA20 on cell viability and ECM production in NHDFs. (**A**) Cell viability of NHDFs treated with indicated concentrations of HA20 (0–0.1%) for 48 h, exhibiting non-significant cytotoxicity within the tested range. (**B**,**C**) Effects of HA20 on the secretion of (**B**) type I collagen and (**C**) elastin in NHDFs, as determined by ELISA. Data are expressed as mean ± SD from three independent experiments. * $p < 0.05$ compared to the control group.

To investigate its potential anti-aging benefits, the key ECM secretion was measured. Treatment with HA20 led to a notable increase in dermal matrix production. Specifically, type I collagen secretion was consistently and significantly higher at all tested concentrations (0.005–0.05%) compared to the control group ($p < 0.05$; Figure 3B). However, the increase did not occur in a strictly concentration-dependent manner. Type I collagen secretion plateaued across the tested concentrations, showing similar levels at both 0.01% and 0.05% HA20. Furthermore, HA20 significantly boosted elastin production, with a particularly strong effect observed at the 0.01% concentration (Figure 3C). Elastin secretion also showed a non-linear pattern, reaching its maximum at 0.01% HA20 rather than increasing steadily at 0.05%. These results show that HA20 effectively promotes ECM synthesis without affecting cell viability. However, its biological activity appears to be limited to an optimal concentration range and does not increase proportionally with higher concentrations.

### *3.4. HA20 Reduced CML Accumulation in Glyoxal-Stimulated NHDFs*

The irreversible accumulation of AGEs, especially CML, plays a key role in skin aging and structural breakdown. To test how HA20 affects glycation, we used immunofluorescence imaging to measure CML levels. Figure 4A,B show that treating NHDFs with 0.5 mM glyoxal caused CML levels to more than double, as seen by the increase in fluorescence intensity compared to the control (Figure 4B, $p < 0.01$). Adding HA20 reduced this glycation-related damage, lowering CML fluorescence to 70.13 ± 24.54% ($p < 0.05$ versus glyoxal). The positive control, AG, nearly eliminated the effect of glyoxal, bringing CML levels down to 44.42 ± 22.74%, which is close to the control value of 42.70 ± 15.36%. These results show that HA20 has a strong anti-glycation effect by reducing AGE formation.

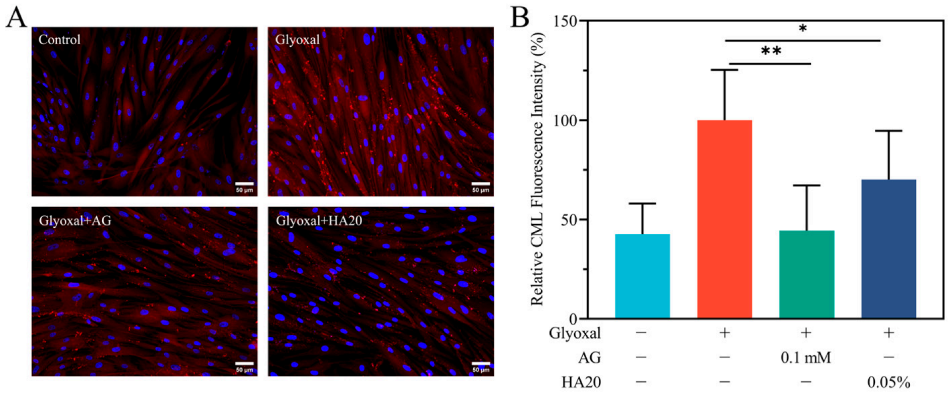



**Figure 4.** HA20 inhibits glyoxal-induced CML accumulation in NHDFs. (**A**) Representative immunofluorescence images of CML (red) and DAPI-stained nuclei (blue). Scale bar = 50 µm. (**B**) Relative fluorescence intensity of CML. The glyoxal-treated group was normalized to 100%. AG served as a positive control. Data are expressed as mean ± SD. ** $p < 0.01$, * $p < 0.05$ versus the glyoxal-treated group.

### *3.5. HA20 Preserved MMP in UVA Irradiation-Exposed NHDFs*

UVA irradiation is a major external factor in dermal photoaging because it disrupts the cellular energy balance [28]. To assess how HA20 protects against UV damage, we measured the MMP (ΔΨm) in NHDFs after UVA exposure using the MitoTracker Deep Red 633 probe. Figure 5 shows that UVA irradiation at 10 J/cm$^2$ greatly reduced mitochondrial function, lowering the MMP to about 59% of the baseline. Treating cells with HA20 before UVA exposure helped prevent this loss. Specifically, 0.1% HA20 almost brought ΔΨm back to normal levels. Interestingly, 0.05% HA20 produced a stronger fluorescence signal than 0.1% HA20, showing that the mitochondrial response to HA20 is not solely based on concentration. This non-linear effect indicates that HA20 may safeguard mitochondrial

function within an optimal concentration range rather than following a straightforward dose–response pattern. These findings imply that HA20 can help preserve mitochondrial integrity and shield dermal fibroblasts from photo-oxidative stress, though further dose–response studies are necessary to pinpoint the most effective concentration.

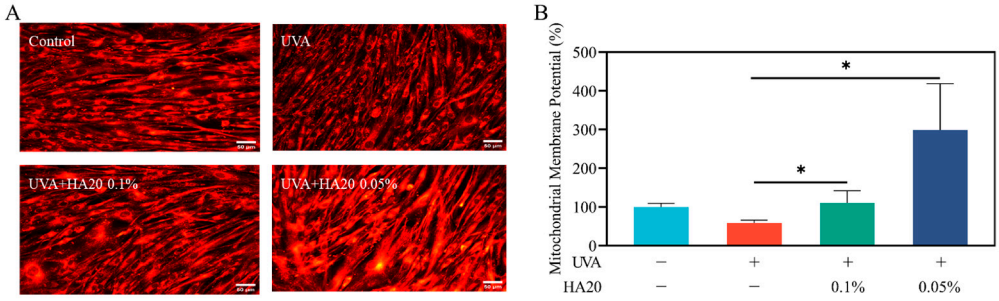



**Figure 5.** HA20 preserves MMP in UVA-irradiated NHDFs. (**A**) Representative fluorescence images exhibiting the MMP in different treatment groups: Control, UVA irradiation, UVA + 0.1% HA20, and UVA + 0.05% HA20. The intensity of red fluorescence represents the MMP level. MMP was assessed using Mito-Tracker Deep Red. Scale bar = 50 μm. (**B**) Quantitative analysis of MMP expressed as a percentage of the control group. Data are presented as mean ± SD. * $p < 0.05$ versus the UVA-irradiated group.

### *3.6. HA20 Suppressed NELL2 and CAII Expression in IL-4/IL-13-Stimulated NHEKs*

AD and sensitive skin are caused by a Th2-driven inflammatory process, mainly involving IL-4 and IL-13 [19,20]. This process damages the skin barrier and leads to intense itching due to abnormal interactions between nerves and the skin. To assess the safety and potential effectiveness of HA20, we first tested its cytotoxicity in NHEKs using the CCK-8 assay. As presented in Figure 6A, HA20 was well tolerated over a wide concentration range (0.0001–0.1%), with cell viability remaining at or above the control levels. Therefore, 0.1% was selected for subsequent functional studies.

To test its soothing effects, NHEKs were placed in an AD-like environment created by IL-4 and IL-13. This treatment led to a significant increase in *NELL2* and *CAII* expression. When 0.1% HA20 was added, it produced a strong and targeted soothing effect. It noticeably reduced *NELL2* expression (Figure 6B, $p < 0.01$) and significantly lowered *CAII* levels (Figure 6C, $p < 0.001$) compared to the stimulated model group. Although inflammatory stress naturally reduced the expression of typical terminal differentiation markers (*FLG* and *LOR*), co-treatment with HA20 did not significantly affect these structural genes under the current stress conditions (Figure 6D,E). These results indicate that HA20 does not act as a typical driver of cornification. Instead, HA20 appears to operate through a specialized regulatory circuit. The findings suggest that its primary role is to silence the neurogenic irritation pathway, which helps ease Th2-mediated inflammatory stress in the skin.

### *3.7. Transcriptomic Profiling and Functional Validation of HA20 in Protecting 3D-RHE Against Extreme Dryness Stress*

To evaluate the comprehensive protective and reparative impacts of HA20 under severe dryness stress, we first performed a histological analysis with H&E staing. Figure 7 shows that acute dryness damaged the structure of 3D-RHE tissue. In the dryness-stressed group, the SC layer was disrupted, with sloughing and detachment from the granular layer. However, tissues treated with HA20 had a compact, organized, and firmly attached SC, similar to the control group. These results suggest that HA20 treatment helped maintain epidermal structure and SC organization during acute dryness stress.

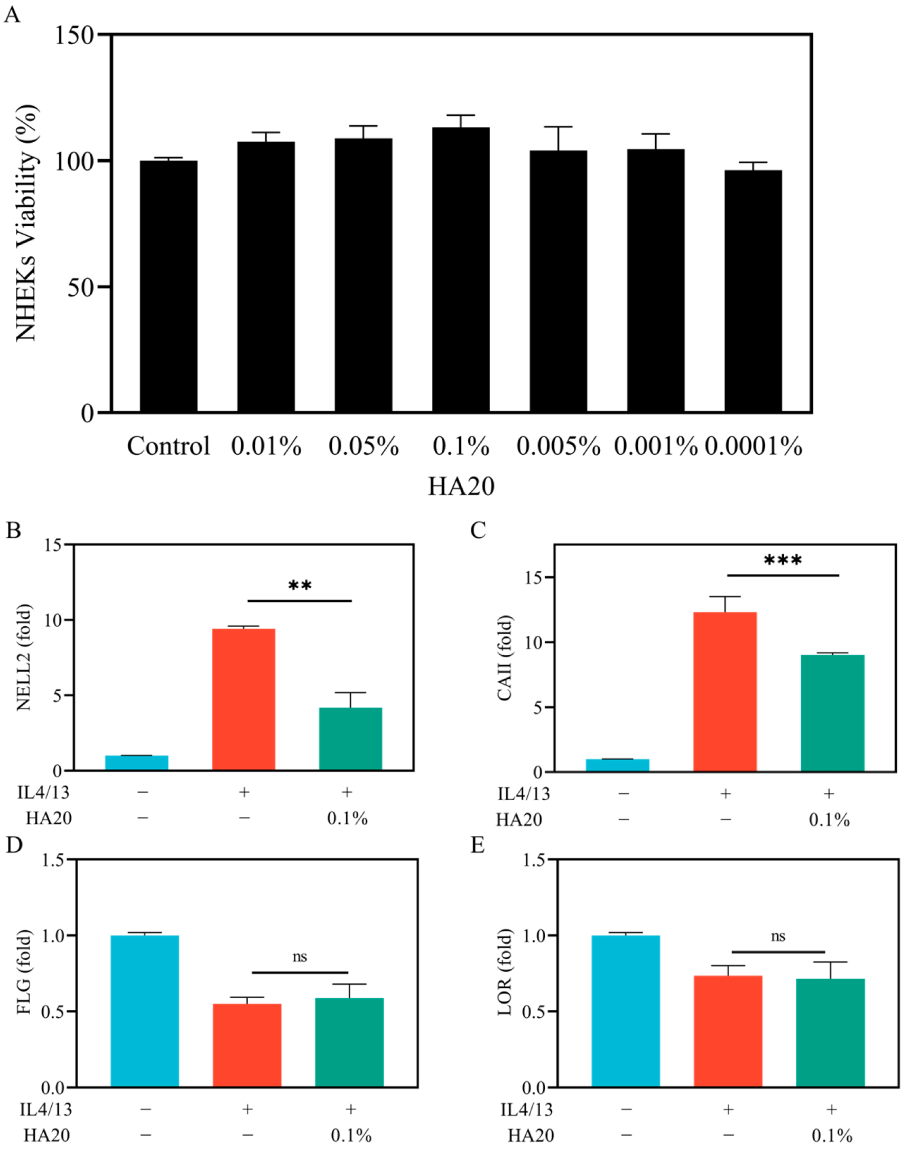



**Figure 6.** HA20 selectively modulates neuro-epidermal stress markers in an IL-4/IL-13-induced AD-like NHEK model. (**A**) Viability of NHEKs treated with the indicated concentrations of HA20. Primary NHEKs were stimulated with a Th2 cytokine cocktail (IL-4 and IL-13, 10 ng/mL each) and concurrently treated with 0.1% HA20 for 72 h. The mRNA expression levels of neurogenic pruritus and stress-associated markers, (**B**) NELL2 and (**C**) CAII, along with terminal differentiation markers, (**D**) FLG and (**E**) LOR, were quantified by RT-qPCR. Data are expressed as mean ± SD. ** $p < 0.01$, *** $p < 0.001$ versus the IL-4/IL-13-stimulated model group; ns, not significant.

To clarify the molecular reasons for these tissue improvements, we performed bulk RNA sequencing on 3D-RHE tissues in three conditions: normal (undisturbed, 50–60% RH), dryness (2 h at less than 20% RH), and HA20 plus dryness (treatment with 0.1% HA20 before dryness exposure). We identified DGEs using volcano plots. Compared to the normal control, dryness stress significantly altered 348 genes (139 up, 209 down; Figure 8A). Notably, topical 0.1% HA20 markedly changed the transcriptomic response under stress, resulting in 305 upregulated and 180 downregulated genes relative to the dryness-treated group (Figure 8B). A Venn diagram analysis showed 71 DEGs shared between both comparisons, suggesting HA20 probably affects a core gene set involved in responding to environmental dehydration (Figure 8C; Table S3).

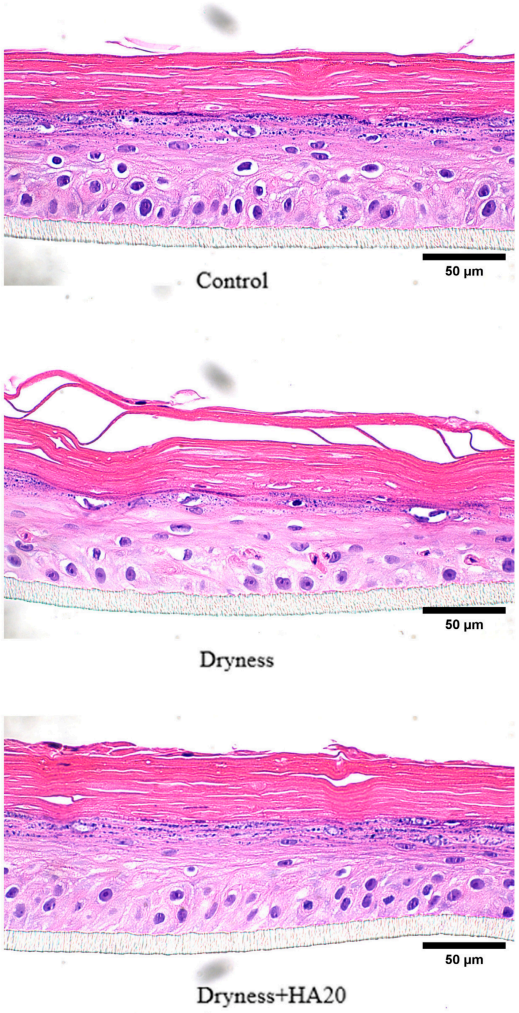



**Figure 7.** Protective effect of HA20 on the epidermal architecture of RHE tissues subjected to acute dryness. Representative images of hematoxylin and eosin-stained sections of RHE tissues under different treatment conditions. All samples were analyzed after a 24 h recovery period. Scale bar = 50 μm.

Functional enrichment analyses, including gene ontology (GO) and Kyoto encyclopedia of genes and genomes (KEGG), indicated that genes affected by HA20 are mainly involved in biological processes related to epidermal homeostasis, such as epidermal development, keratinocyte differentiation, and keratinization (Figure 8D). Cellular component analysis showed that collagen-containing ECM and basement membranes were significantly enriched. KEGG analysis also highlighted the activation of pathways like focal adhesion, PI3K-AKT signaling, and ECM-receptor interactions, which are important for structural stability and cell survival during barrier repair. The PI3K-AKT pathway is important for cell survival, proliferation, and differentiation, which are needed for keratinocyte function and skin healing. Focal adhesion and ECM-receptor interaction pathways are also key for cell–matrix interactions, helping maintain dermo-epidermal cohesion and support tissue regeneration.

To validate these gene expression results, we used RT-qPCR to measure four key markers: *KRT37*, *COL7A1*, *ACER2*, and *SPRR1A* (Figure 8E–H). Dryness stress lowered the expression of *SPRR1A* and *ACER2* ($p < 0.05$), but treating with 0.1% HA20 reversed this and increased their levels (all $p < 0.05$). HA20 also raised the expression of *KRT37* and *COL7A1* (both $p < 0.05$). Overall, these findings show that HA20 helps repair tissue by restoring

structure, supporting keratinocyte differentiation, and strengthening the dermal-epidermal junction under harsh conditions.

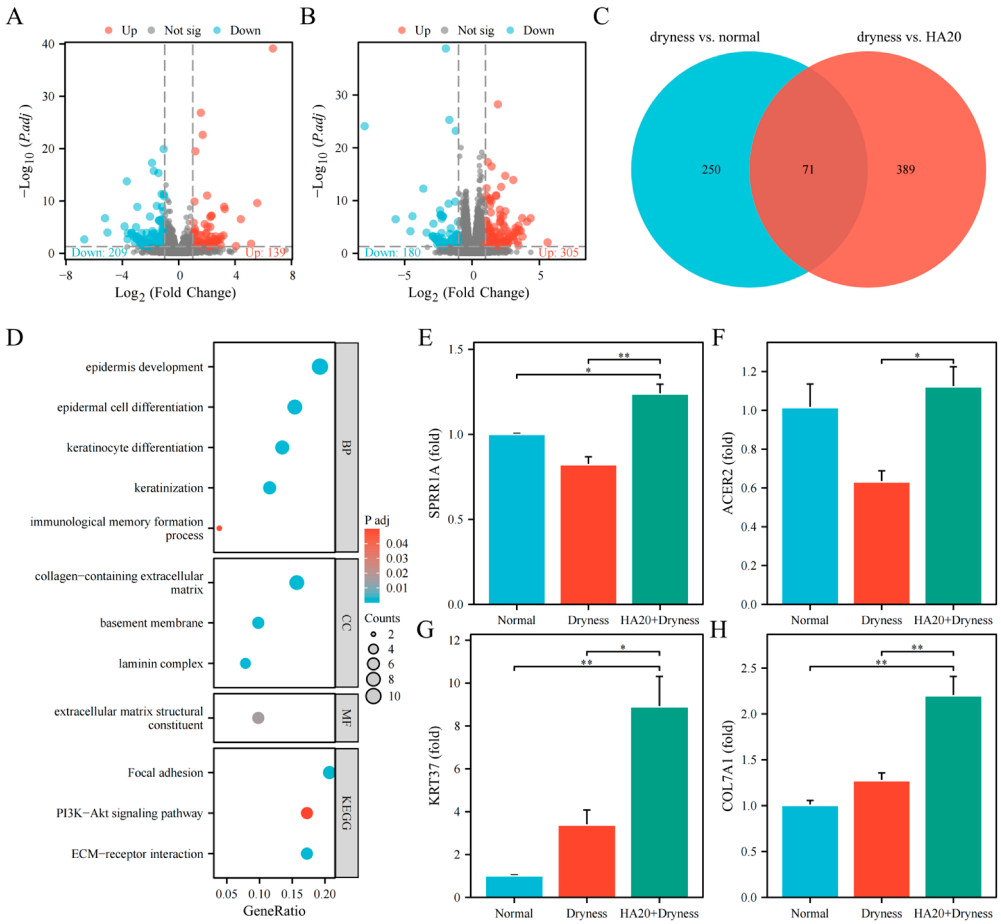



**Figure 8.** Transcriptomic analysis and qPCR validation of the effects of HA20 on 3D RHE under dryness stress. (**A**,**B**) Volcano plots exhibiting DEGs in (**A**) Dryness versus normal and (**B**) HA20 + dryness versus dryness comparisons. Red and blue dots represent significantly up- and down-regulated genes, respectively (adjusted $p < 0.05$, $|\log_2 FC| > 1.2$). The horizontal dashed line indicates the adjusted p-value threshold, and the vertical dashed lines indicate the $|\log_2 FC|$ thresholds used to identify DEGs. (**C**) Venn diagram illustrating the 71 common DEGs between the two comparison groups. (**D**) Functional enrichment analysis (GO and KEGG) of DEGs modulated by HA20. The dot size represents the gene count, and the color indicates the adjusted p-value. (**E**–**H**) RT-qPCR validation of representative markers involved in cornification ((**E**), *SPRR1A*), lipid metabolism ((**F**), *ACER2*), keratinization ((**G**), *KRT37*), and basement membrane integrity ((**H**), *COL7A1*). Data are presented as mean ± SD. * $p < 0.05$, ** $p < 0.01$ versus the dryness-stressed group.

## 4. Discussion

The present study was designed to address the HA MW paradox, which describes the complex relationship between HA molecular size and its biological effects. High-MW HA typically supports tissue homeostasis, reduces inflammation, modulates immunity, retains hydration, and strengthens barriers. Conversely, low-MW HA or oligomers are more mobile and accessible to receptors, often initiating repair processes, proliferation, angiogenesis, or inflammation, depending on the biological environment [5–7]. This study thoroughly assessed the multi-dimensional defensive and reparative effects of HA20—a carefully designed broad-spectrum HA complex ($M_W$ approximately 200 kDa; size range 10–1000 kDa)—against various skin exposome stressors. Our findings show that HA20 offers improved transepidermal bioavailability compared with high-MW HA. At the dermal

level, HA20 strongly promoted type I collagen and elastin production, and it has significant photoprotective and anti-glycation effects. These findings offer strong experimental evidence that topically applied HA can directly reduce glyoxal-induced CML accumulation, filling a clear gap in dermatological research. Within the epidermis, HA20 exerted its effects by specifically suppressing the expression of Th2-driven, pruritus-associated keratinocyte markers. It also ensured the structural barrier integrity during severe dryness by modulating the expression of certain genes. Overall, these results show that the broad-spectrum MW distribution of HA20 helps balance surface barrier support with deeper skin signaling. This allows HA20 to serve as a multifunctional exposome-defense active, promoting dermal matrix remodeling and enhancing epidermal barrier resilience.

The improved biological performance of HA20 may stem from its wide molecular weight distribution, which leads to increased bioactivity. In the RHE permeation model, HA20 showed higher ELISA-detectable apparent cumulative permeation and a faster onset compared to high-MW HA (Figure 2). Additionally, a preliminary in vivo Raman spectroscopy study indicated that HA20 had higher skin penetration than high-MW HA over 2–10 h (Figure S1; Tables S1 and S2). However, this finding is considered preliminary since only three volunteers participated. Together, the RHE and pilot Raman findings support the hypothesis of a stratified penetration mechanism, which is supported by the fact that HA20 has polydisperse properties, allowing for a more effective and continuous flux through the skin layers. This study examined HA20 as a complete complex, but it has a strong stimulation effect on Type I collagen and elastin (Figure 3), which is probably because it has a variety of MW components. In particular, lower-MW fragments are included, which may contribute to enhanced penetration within the skin, and there are approximately 200 kDa "transition-size" signaling nodes, which promote fibroblast activation [7]. The polydisperse structure of HA20 reduces typical physiological issues related to isolated MW fractions.

Importantly, the polydisperse composition of HA20 helps avoid the physiological issues often seen with single-size HA. While pure low-MW HA has been reported to potentially increase transepidermal water loss [10], results from the RHE model indicate that HA20 supports epidermal structure rather than causing damage, even when the skin is under severe dryness stress. These findings suggest that the higher-MW components of HA20 provide structural support and maintain skin hydration, balancing the drying effects of smaller fragments. By reinforcing the skin's surface and rejuvenating deeper layers, HA20 delivers a more comprehensive protective effect than single-size HA. This combination establishes a strong physical and biological foundation for defending the skin against environmental stressors.

At the dermal level, HA20 has a strong ability to protect the skin from oxidative stress and glycation, which are major drivers of skin exposome damage. A key result of this study is the clear evidence that HA20 significantly reduces CML accumulation in NHDFs (Figure 4). These results align with recent ex vivo studies on HA-based systems [29]. A dual-weight HA formulation with trehalose was found to reduce CML formation by up to 69% in a methylglyoxal-stimulated human skin model [29]. Although this study employed an invasive injectable delivery method and used trehalose as a stabilizer, our data show that the broad-spectrum HA complex HA20 alone can effectively reduce CML accumulation within cells. By inhibiting CML deposition, HA20 maintains the flexibility and durability of newly formed collagen and elastin fibers, as shown in our ECM assays (Figure 3). These findings suggest that HA20 provides a comprehensive approach to increase matrix production and prevent breakdown caused by glycation.

Additionally, HA20 helps prevent photoaging by maintaining mitochondrial stability. UVA radiation accelerates skin aging partly by rapidly reducing MMP ($\Delta\Psi m$), indicat-

ing a disruption in energy production [14]. Our results indicate that 0.1% HA20 restores UVA-induced reductions in MMP levels close to control values, while 0.05% HA20 more strongly enhances MitoTracker Deep Red fluorescence (Figure 5). This non-linear response suggests that HA20 may act within an optimal concentration window rather than exhibiting a linear, dose-dependent effect. A comparable pattern appeared in the ECM secretion assay: Type I collagen secretion plateaued across tested HA20 concentrations, and elastin secretion peaked at 0.01% HA20 rather than increasing with higher concentrations. Consequently, both ECM and mitochondrial markers demonstrate that HA20 improves dermal cell function within an effective concentration range, but the response does not increase proportionally with concentration. This window-specific effect may be linked to the polydisperse nature of HA20. Because HA20 is a broad-MW HA complex, its activity may depend on the balance among MW distribution, local cellular availability, receptor engagement, and signaling saturation. This interpretation is supported by previous reports showing that the antioxidant behavior of HA is concentration- and environment-dependent. Moriya reported that low-MW HA directly scavenges hydroxyl radicals, but its activity does not increase proportionally across a 10-fold concentration range [30]. Rapta et al. further found that high-MW HA's radical-scavenging behavior depends on the assay system, concentration, reaction medium, and ionic environment, showing effective scavenging at lower concentrations but more complex responses at higher concentrations or specific ionic conditions [31]. Thus, the stronger response at 0.05% HA20 compared to 0.1% HA20 should be interpreted with caution as a non-linear biological response. Additional dose–response studies are needed to determine the optimal HA20 concentration in UVA-induced oxidative stress models.

Besides dermal matrix remodeling and mitochondrial protection, this study also indicates that HA20 can modulate epidermal inflammation. The present study demonstrates that 0.1% HA20 selectively reduces the expression of pruritus-related markers *NELL2* and *CAII* in NHEKs when they are stimulated by IL-4 and IL-13. These findings offer new understanding of HA's role in Th2-driven inflammatory skin conditions. The results show that Th2 cytokines (IL-4 and IL-13) directly increase *NELL2* and *CAII* expression in an in vitro AD-like setting, which supports the idea of neuro-epidermal crosstalk in chronic pruritus [19,21]. HA20's ability to block this effect suggests it may act as a bioactive antagonist against neurogenic itch signaling caused by Th2 inflammation. This matches clinical findings in prurigo nodularis, where lesions often show strong STAT6 activation and high HA accumulation [32]. These results suggest that HA accumulation might not just be a byproduct of disease, but could also help regulate it. It seems to reduce ongoing Th2-driven stress by lowering pruritogenic mediators like *NELL2* and *CAII*.

It is important to highlight that HA20 is highly specific. HA20 reduced neurogenic markers, but did not reverse IL-4/IL-13-driven suppression of terminal differentiation markers such as *FLG* and *LOR*. This means that, in this acute inflammatory model, HA20 does not mainly enhance differentiation. Instead, it has a targeted effect on the neurogenic itch cycle. This selectivity makes HA20 different from broad-spectrum barrier repair products and supports a precision medicine approach aimed at easing sensory skin symptoms rather than only repairing the skin barrier.

Consistent with the cell-level findings, the 3D-RHE dryness model offered tissue-level evidence linking HA20's apparent bioavailability and cellular activity to barrier protection. This study shows that, in an acute, extreme dryness-stressed 3D skin model, HA20 helps maintain skin barrier integrity through multi-dimensional, genome-level regulation. This mechanism goes beyond its typical function as a passive humectant. Histological analysis gave a strong indication of this protective effect. While the control group exhibited severe structural disorganization, HA20 treatment maintained SC as compact, well-stratified, and

closely adherent. These results broaden our understanding of HA, suggesting its role not only in managing chronic photoaging or xerosis [33,34] but also in supporting quick defense and structural repair against sudden environmental damage.

Our main evidence shows that HA20 precisely regulates a set of key genes, which are crucial for maintaining epidermal balance. Dryness stress significantly reduced the expression of *SPRR1A* and *ACER2*, which is consistent with in vivo findings showing that dry skin often correlates with lower expression of barrier-related genes [35]. HA20 treatment reversed this downregulation and significantly increased *KRT37* and *COL7A1* levels. This indicates a complex protective mechanism: higher *KRT37* levels, as a member of the keratin family, probably strengthen the keratinocyte cytoskeleton. This strengthening enhances mechanical resilience against desiccation stress [36] and supports the stability of the epidermal structure. At the same time, the increase in *COL7A1*—which encodes the key component of anchoring fibrils at the dermal-epidermal junction (DEJ) [37]—suggests that HA actively strengthens the skin's deeper structural framework to prevent epidermal sloughing under stress. This result matches previous studies showing that HA helps remodel the ECM and supports collagen production, which improves skin integrity [38]. Also, the increase in *ACER2* points to its important role in ceramide metabolism, which is essential for keeping the lipid barrier that controls water retention [39]. The increase in *SPRR1A* at the same time suggests that HA supports terminal differentiation, leading to a stronger and more durable cornified envelope [40]. This matches the dense, cohesive structure of the SC seen under the microscope.

Pathway enrichment analysis showed that the PI3K-AKT, focal adhesion, and ECM-receptor interaction pathways are key signaling centers that HA20 uses to control gene expression for structural repair. These pathways influence cell survival, growth, differentiation, and interactions with the extracellular matrix. The findings suggest that during acute dryness, HA20 activates these important networks to strengthen the barrier, support cytoskeletal stability, repair lipid metabolism, and promote terminal differentiation and DEJ stabilization.

The current findings both confirm and expand upon previous research. While many studies have demonstrated that increasing natural HA levels [41] or taking oral HA supplements [33] can enhance skin hydration in chronic conditions, our study is distinctive because it focuses on acute dryness. We show that topically applied HA rapidly induces transcriptomic changes that directly regulate downstream effector genes associated with structural integrity and metabolic stability, confirming its ability to provide rapid histological protection.

Overall, the broad MW distribution of HA20 appears to be a major advantage. Evidence indicates that different MWs of HA provide complementary effects: medium- to -high MW HA offers structural support and surface hydration [33], while low-MW HA enhances tissue penetration and signaling, affecting deeper dermal functions [42]. Recent proteomic and lipidomic studies report that treating human dermal fibroblasts with 20–50 kDa HA boosts collagen production, reorganizes the ECM, and increases ceramide synthesis [43,44]. These metabolic changes are consistent with the higher levels of *COL7A1* and *ACER2* expression observed in this study. Because HA20 contains a wide range of MW, it can use the benefits of different HA fractions. This multi-target approach activates a connected signaling network that affects epidermal differentiation, barrier lipid metabolism, and remodeling of the deeper dermal matrix. Together, these actions help support strong and coordinated barrier defense and tissue repair. These results could lead to new HA-based treatments for acute skin barrier damage.

This study successfully shows that HA20 has several protective and repair effects against the skin exposome, but there are some limitations. First, while the RHE model

gives a detailed look at epidermal barrier function and gene expression, it does not capture the full complexity of living tissues. As a result, the lack of validation in living organisms limits the direct application of our results to actual physiological or disease conditions. Furthermore, while the 2D NHEK monolayer system offered a controlled environment for examining IL-4/IL-13-induced neurogenic stress markers, validating these findings in a structurally intact 3D reconstructed epidermal model would enhance their significance at the tissue level. Second, regarding mechanistic insights, although transcriptomic profiling showed that HA20 triggers vital survival and structural pathways—such as PI3K-AKT and focal adhesion—in response to dryness stress, we did not conduct gene silencing (siRNA) experiments to establish a direct causal link between specific receptors and the observed effects. In addition, we did not validate key signaling proteins at the protein level, such as checking phosphorylation states, which limits our understanding of HA20's molecular mechanisms. Third, the current dryness experiment lacked a control group matched with moisturizer or humectant. While histological and transcriptomic findings indicate that HA20 protects against acute dryness stress, future research should include appropriate moisturizing controls to clearly distinguish HA20's specific biological effects from general moisturizing benefits. Fourth, the experiment was an acute stress-recovery model with 2 h of severe dryness followed by 24 h of recovery. This short timeframe is effective for early detection of morphological and stress-related transcriptomic changes but may not be enough to observe significant protein-level changes in late differentiation markers like filaggrin and loricrin. Longer studies, including recovery days 3, 5, and 7, are necessary to more accurately assess late-stage epidermal differentiation and cornified-envelope restructuring. Fifth, the ELISA-based RHE permeation assay only detects HA within the $\geq$35 kDa range, potentially underestimating HA20 permeation since it includes fractions below 35 kDa. Larger sample size studies using Raman spectroscopy are necessary to verify the in vivo skin penetration profile of HA20. Sixth, although HA20 showed stronger apparent performance than single-MW HA controls, we did not include a physically blended HA mixture with the same MW distribution as a control. Therefore, it remains difficult to determine whether the observed benefits arise from synergistic effects among different MW fractions, from the specific manufacturing process of HA20, or from additive effects of individual HA components. Finally, all efficacy assessments were performed using acute or short-term stress models. We did not examine how HA20 affects skin barrier remodeling after long-term use, nor did we evaluate potential long-term safety issues or how well HA20 maintains its stability and bioactivity in finished cosmetic products. These are important gaps that require further research.

Future research should continue to validate broad-MW HA systems in more translational contexts. Specifically, longer-term ex vivo and clinical studies are necessary to see if the initial histological and transcriptomic responses observed here lead to lasting improvements in hydration, transepidermal water loss, barrier recovery, elasticity, wrinkle-related parameters, and subjective symptoms. Comparative studies involving defined single-MW HA fractions, physically blended HA mixtures, and HA20 with matched MW distributions could help determine whether its activity is additive, synergistic, or process-dependent. Mechanistic experiments focusing on candidate HA receptors, along with protein-level validation of pathways such as PI3K-AKT, focal adhesion, ECM-receptor interaction, mitochondrial stress, and differentiation, would further clarify causal relationships. Finally, incorporating moisturizer-matched controls, finished formulations, and multi-stressor exposome models can better evaluate the practical relevance of broad-MW HA complexes as barrier-protective and skin-resilience ingredients.

## 5. Conclusions

This study found that HA20, a specially designed broad-spectrum HA complex (Mw ~200 kDa; range 10–1000 kDa), works as a multi-targeted defense against environmental stressors, helping to protect and repair different layers of the skin. Its mix of molecule sizes improves how well it penetrates the skin and supports various biological functions. In the dermis, HA20 helps reduce signs of aging by increasing collagen I and elastin production. It also lowers glyoxal-induced CML buildup and helps keep MMP stable during UVA-related damage. In the epidermis, HA20 shows targeted effects by reducing neurogenic itch markers (*NELL2*, *CAII*) triggered by IL4/IL3 cytokines and, in very dry conditions, starting a rescue program at the gene level. This program, which involves the PI3K-AKT and focal adhesion pathways, increases the activity of important barrier genes (*KRT37*, *COL7A1*, *ACER2*, *SPRR1A*) to support skin structure and lipid metabolism, helping to maintain the stratum corneum. Overall, these results show that HA20 is more than just a moisturizer. HA20 acts as an active ingredient that links surface hydration with deeper skin renewal. By targeting glycation, photo-oxidation, neurogenic inflammation, and dehydration together, HA20 offers strong scientific support for advanced skincare formulations that meet the complex needs of skin health.

**Supplementary Materials:** The following supporting information can be downloaded at https://www.mdpi.com/article/10.3390/cosmetics13040179/s1, Supplementary Methods and Results: Exploratory in vivo Raman spectroscopy assessment of relative skin penetration after topical application of high-MW HA and HA20; Supplementary Transcriptomic Data: The 71 core DEGs shared between the two transcriptomic comparisons. Figure S1: Depth-resolved distribution images of characteristic Raman signals for (A) high-MW HA and (B) HA20 in human skin at 0, 2, 4, 8, and 10 h after topical application; Table S1: Relative penetration rate of high-MW HA and HA20 in human skin at different time points measured by exploratory in vivo Raman spectroscopy ($n$ = 3); Table S2: Maximum penetration depth of high-MW HA and HA20 in human skin at different time points measured by exploratory in vivo Raman spectroscopy ($n$ = 3); Table S3: List of 71 core differentially expressed genes (DEGs) co-modulated by dryness stress and HA20 treatment in 3D-RHE models.

**Author Contributions:** Conceptualization, Z.W. and P.L.; methodology, Z.W., Y.F., L.Z. and D.J.; software, Y.F. and D.J.; validation, L.Z., D.J. and Z.W.; formal analysis, Y.F. and D.J.; investigation, Y.F., L.Z., J.Q., D.J. and Z.W.; resources, Z.W., L.Z. and P.L.; data curation, Y.F. and D.J.; writing—original draft preparation, Z.W.; writing—review and editing, Y.F., L.Z., J.Q., D.J. and P.L.; visualization, Y.F., J.Q. and D.J.; supervision, Z.W. and P.L.; project administration, P.L.; funding acquisition, Z.W. All authors have read and agreed to the published version of the manuscript.

**Funding:** This research received no external funding.

**Institutional Review Board Statement:** Not applicable.

**Informed Consent Statement:** Not applicable.

**Data Availability Statement:** The datasets generated and analyzed during the current study are available in the article and its Supplementary Materials (Figure S1 and Tables S1–S3). The raw datasets (including individual physiological data) are not publicly available due to privacy restrictions but are available from the corresponding authors on reasonable request.

**Acknowledgments:** Grammarly was used solely for grammar, spelling, punctuation, and language polishing.

**Conflicts of Interest:** Z.W., Y.F. and J.Q. are employed by Meyer Bio-Medicine Co., Ltd. L.Z. and D.J. are employed by Shanghai Archgene Biotechnology Co., Ltd. The remaining author declares that the research was conducted in the absence of any commercial or financial relationships that could be construed as a potential conflict of interest. The authors declare no other conflicts of interest.

## Abbreviations

The following abbreviations are used in this manuscript:

| | |
|---|---|
| HA | Hyaluronic Acid |
| ECM | Extracellular Matrix |
| MW | Molecular Weight |
| SC | Stratum Corneum |
| UV | Ultraviolet |
| AGEs | Advanced Glycation End-Products |
| CML | NE-(Carboxymethyl)Lysine |
| AD | Atopic Dermatitis |
| IL | Interleukin |
| CCK-8 | Cell Counting Kit-8 |
| RHE | Reconstructed Human Epidermis |
| AG | Aminoguanidine |
| MMP | Mitochondrial Membrane Potential |
| GPC | Gel Permeation Chromatography |
| NHDFs | Normal Human Dermal Fibroblasts |
| NHEKs | Normal Human Epidermal Keratinocytes |
| PCR | Polymerase Chain Reaction |
| RH | Relative Humidity |
| DEGs | Differentially Expressed Genes |
| Mw | Weight-Average Molecular Weight |
| Mn | Number-Average Molecular Weight |
| Mp | Peak Molecular Weight |
| GO | Gene Ontology |
| KEGG | Kyoto Encyclopedia Of Genes And Genomes |
| DEJ | Dermal-Epidermal Junction |
| CAII | Carbonic Anhydrase Ii |
| NELL2 | Neural Egfl Like 2 |
| FLG | Filaggrin |
| LOR | Loricrin |
| KRT37 | Keratin 37 |
| COL7A1 | Collagen Type Vii Alpha 1 Chain |
| ACER2 | Alkaline Ceramidase 2 |
| SPRR1A | Small Proline Rich Protein 1a |

## References

1. Juncan, A.M.; Moisă, D.G.; Santini, A.; Morgovan, C.; Rus, L.-L.; Vonica-Țincu, A.L.; Loghin, F. Advantages of Hyaluronic Acid and Its Combination with Other Bioactive Ingredients in Cosmeceuticals. *Molecules* **2021**, *26*, 4429. [CrossRef] [PubMed]
2. Žádníková, P.; Šínová, R.; Pavlík, V.; Šimek, M.; Šafránková, B.; Hermannová, M.; Nešporová, K.; Velebný, V. The Degradation of Hyaluronan in the Skin. *Biomolecules* **2022**, *12*, 251. [CrossRef] [PubMed]
3. Galvan, A.; Lacavalla, M.A.; Boschi, F.; Cisterna, B.; Dalla Pozza, E.; Vigato, E.; Carton, F.; Malatesta, M.; Calderan, L. A Fluid Dynamic In Vitro System to Study the Effect of Hyaluronic Acid Administration on Collagen Organization in Human Skin Explants. *Int. J. Mol. Sci.* **2025**, *26*, 5397. [CrossRef] [PubMed]
4. Chylińska, N.; Maciejczyk, M. Hyaluronic Acid and Skin: Its Role in Aging and Wound-Healing Processes. *Gels* **2025**, *11*, 281. [CrossRef] [PubMed]
5. Wang, X.; Liu, X.; Li, C.; Li, J.; Qiu, M.; Wang, Y.; Han, W. Effects of Molecular Weights on the Bioactivity of Hyaluronic Acid: A Review. *Carbohydr. Res.* **2025**, *552*, 109472. [CrossRef]
6. Cho Lee, A.R. Size Matters: Differential Property of Hyaluronan and Its Fragments in the Skin- Relation to Pharmacokinetics, Immune Activity and Wound Healing. *J. Pharm. Investig.* **2023**, *53*, 357–376. [CrossRef]
7. Giardina, S.; Poggi, A. Skin Penetration Ability of 12 Hyaluronic Acids with Different Molecular Weights After Topical Application. *JOJ Dermatol. Cosmet.* **2023**, *5*, 555665. [CrossRef]

8. Essendoubi, M.; Gobinet, C.; Reynaud, R.; Angiboust, J.F.; Manfait, M.; Piot, O. Human Skin Penetration of Hyaluronic Acid of Different Molecular Weights as Probed by Raman Spectroscopy. *Ski Res. Technol.* **2016**, *22*, 55–62.
9. Stephanie, W.; Elliott, L.; Todd, S. Update on Low-Molecular Weight Hyaluronic Acid in Dermatology: A Scoping Review. *EMJ Dermatol.* **2024**, *12*, 134–146. [CrossRef]
10. Sundaram, H.; Mackiewicz, N.; Burton, E.; Peno-Mazzarino, L.; Lati, E.; Meunier, S. Pilot Comparative Study of the Topical Action of a Novel, Crosslinked Resilient Hyaluronic Acid on Skin Hydration and Barrier Function in a Dynamic, Three-Dimensional Human Explant Model. *J. Drugs Dermatol.* **2016**, *15*, 434–441. [PubMed]
11. Park, H.Y.; Kweon, D.K.; Kim, J.K. Upregulation of Tight Junction-Related Proteins by Hyaluronic Acid in Human HaCaT Keratinocytes. *Bioact. Carbohydr. Diet. Fibre* **2023**, *30*, 100374. [CrossRef]
12. Ito, S.; Kurihara, H.; Kuriyama, K.; Kimura, M.; Tokudome, Y. 2 kDa Hyaluronic Acid Reduces Blemishes and Sagging in Human Facial Skin. *Clin. Cosmet. Investig. Dermatol.* **2025**, *18*, 805–816. [CrossRef] [PubMed]
13. Passeron, T.; Krutmann, J.; Andersen, M.L.; Katta, R.; Zouboulis, C.C. Clinical and Biological Impact of the Exposome on the Skin. *J. Eur. Acad. Dermatol. Venereol.* **2020**, *34*, 4–25. [CrossRef] [PubMed]
14. Battie, C.; Jitsukawa, S.; Bernerd, F.; Del Bino, S.; Marionnet, C.; Verschoore, M. New Insights in Photoaging, UVA Induced Damage and Skin Types. *Exp. Dermatol.* **2014**, *23*, 7–12. [CrossRef] [PubMed]
15. Zhou, H.; Zhou, L.; Li, B.; Yue, R. Anti-Cyclooxygenase, Anti-Glycation, and Anti-Skin Aging Effect of Dendrobium Officinale Flowers' Aqueous Extract and Its Phytochemical Validation in Aging. *Front. Immunol.* **2023**, *14*, 1095848. [CrossRef] [PubMed]
16. Pageon, H.; Bakala, H.; Monnier, V.M.; Asselineau, D. Collagen Glycation Triggers the Formation of Aged Skin In Vitro. *Eur. J. Dermatol.* **2007**, *17*, 12–20. [CrossRef] [PubMed]
17. Oetjen, L.K.; Mack, M.R.; Feng, J.; Whelan, T.M.; Niu, H.; Guo, C.J.; Chen, S.; Trier, A.M.; Xu, A.Z.; Tripathi, S.V.; et al. Sensory Neurons Co-opt Classical Immune Signaling Pathways to Mediate Chronic Itch. *Cell* **2017**, *171*, 217–228.e13. [CrossRef] [PubMed]
18. Engebretsen, K.A.; Johansen, J.D.; Kezic, S.; Linneberg, A.; Thyssen, J.P. The Effect of Environmental Humidity and Temperature on Skin Barrier Function and Dermatitis. *J. Eur. Acad. Dermatol. Venereol.* **2016**, *30*, 223–249. [PubMed]
19. Egawa, G.; Kabashima, K. Multifactorial Skin Barrier Deficiency and Atopic Dermatitis: Essential Topics to Prevent the Atopic March. *J. Allergy Clin. Immunol.* **2016**, *138*, 350–358.e1. [CrossRef] [PubMed]
20. Ständer, S. Atopic Dermatitis. *N. Engl. J. Med.* **2021**, *384*, 1136–1143. [CrossRef] [PubMed]
21. Mack, M.R.; Kim, B.S. The Itch-Scratch Cycle: A Neuroimmune Perspective. *Trends Immunol.* **2018**, *39*, 980–991. [CrossRef] [PubMed]
22. Chmielewski, R.; Lesiak, A. Mitigating Glycation and Oxidative Stress in Aesthetic Medicine: Hyaluronic Acid and Trehalose Synergy for Anti-AGEs Action in Skin Aging Treatment. *Clin. Cosmet. Investig. Dermatol.* **2024**, *17*, 2701–2712. [CrossRef] [PubMed]
23. Ling, P.; Shao, H.; Zeng, Q. A Sodium Hyaluronate with Full Molecular Weight Distribution and Its Preparation Method and Application. Chinese Patent ZL 2021 10874694.1, 20 May 2022. [CrossRef] [PubMed]
24. Chinese Pharmacopoeia Commission. General Rule 1143: Bacterial Endotoxins Test. In *Chinese Pharmacopoeia (2020 Edition)*; China Medical Science Press: Beijing, China, 2020; Volume IV.
25. Hao, F.; Jin, X.; Liu, Q.S.; Zhou, Q.; Jiang, G. Epidermal Penetration of Gold Nanoparticles and Its Underlying Mechanism Based on Human Reconstructed 3D Episkin Model. *ACS Appl. Mater. Interfaces* **2017**, *9*, 42577–42588. [CrossRef] [PubMed]
26. Agonia, A.S.; Palmeira-de-Oliveira, A.; Cardoso, C.; Augusto, C.; Pellevoisin, C.; Videau, C.; Dinis-Oliveira, R.J.; Palmeira-de-Oliveira, R. Reconstructed Human Epidermis: An Alternative Approach for In Vitro Bioequivalence Testing of Topical Products. *Pharmaceutics* **2022**, *14*, 1554. [CrossRef] [PubMed]
27. Viodé, C.; Rouquier, A.; Mias, C.; Questel, E.; Bessou-Touya, S.; Duplan, H. Specific Protection of Sensitive Skin Against Environmental Stress by Maintenance and Improvement of Barrier Function. *J. Eur. Acad. Dermatol. Venereol.* **2022**, *36*, 13–20. [CrossRef] [PubMed]
28. Niccolini, B.; Riente, A.; Hatem, D.; Bottoni, P.; Pizzoferrato, M.; Tringali, G.; Tabolacci, E.; Maulucci, G.; Marini, S.; Ciaccio, C.; et al. Polydatin Prevents UVA-Induced Damage in Human Dermal Fibroblasts by Maintaining Mitochondrial Integrity. *Cells* **2025**, *14*, 1702. [CrossRef] [PubMed]
29. Chmielewski, R.; Lebiedowska, A.; Barańska-Rybak, W. Assessment of the Curative Anti-Glycation Properties of a Novel Injectable Formulation Combining Dual-Weight Hyaluronic Acid (Low- and Mid/High-Molecular Weight) with Trehalose on Human Skin Ex Vivo. *Int. J. Mol. Sci.* **2025**, *26*, 4747. [CrossRef] [PubMed]
30. Moriya, M. Enhanced radical scavenging activity by interactions between hyaluronan and antioxidants—A study of hyaluronan-containing drinks. *Food Sci. Technol. Res.* **2022**, *28*, 159–168. [CrossRef]
31. Rapta, P.; Valachová, K.; Gemeiner, P.; Soltés, L. High-molar-mass hyaluronan behavior during testing its radical scavenging capacity in organic and aqueous media: Effects of the presence of manganese(II) ions. *Chem. Biodivers.* **2009**, *6*, 162–169. [CrossRef] [PubMed]

32. Fukushi, S.; Yamasaki, K.; Aiba, S. Nuclear Localization of Activated STAT6 and STAT3 in Epidermis of Prurigo Nodularis. *Br. J. Dermatol.* **2011**, *165*, 990–996. [CrossRef] [PubMed]
33. Kawada, C.; Kimura, M.; Masuda, Y.; Nomura, Y. Oral Administration of Hyaluronan Prevents Skin Dryness and Epidermal Thickening in Ultraviolet Irradiated Hairless Mice. *J. Photochem. Photobiol. B* **2015**, *153*, 215–221. [CrossRef] [PubMed]
34. Kawada, C.; Kimura, M.; Masuda, Y.; Nomura, Y. Orally Administered Hyaluronan Affects Skin Dryness and Epidermal Thickening in Photoaged Hairless Mice. *Biosci. Biotechnol. Biochem.* **2016**, *80*, 1192–1195. [CrossRef] [PubMed]
35. Shinozaki, Y.; Ikarashi, N.; Tabata, K.; Miyazawa, A.; Kon, R.; Sakai, H.; Hosoe, T. Expression Analysis of Genes Important for Maintaining Skin Function in a Senescence-Accelerated Mouse Prone Model. *Geriatr. Gerontol. Int.* **2023**, *23*, 951–957. [CrossRef] [PubMed]
36. Chen, J.; Liu, C.; Yang, Y.; Gong, X.; Qian, H. The Stratum Corneum Barrier: Impaired Function in Relation to Associated Lipids and Proteins. *Tissue Barriers* **2025**, *13*, 2361197. [PubMed]
37. De Gregorio, C.; Catalán, E.; Garrido, G.; Morandé, P.; Bennett, J.C.; Muñoz, C.; Cofré, G.; Huang, Y.L.; Cuadra, B.; Murgas, P.; et al. Maintenance of Chronicity Signatures in Fibroblasts Isolated from Recessive Dystrophic Epidermolysis Bullosa Chronic Wound Dressings under Culture Conditions. *Biol. Res.* **2023**, *56*, 23. [CrossRef] [PubMed]
38. Stellavato, A.; Corsuto, L.; D'Agostino, A.; La Gatta, A.; Diana, P.; Bernini, P.; De Rosa, M.; Schiraldi, C. Hyaluronan Hybrid Cooperative Complexes as a Novel Frontier for Cellular Bioprocesses Re-Activation. *PLoS ONE* **2016**, *11*, e0163510. [CrossRef] [PubMed]
39. Nădăban, A.; Rousel, J.; El Yachioui, D.; Gooris, G.S.; Beddoes, C.M.; Dalgliesh, R.M.; Malfois, M.; Rissmann, R.; Bouwstra, J.A. Effect of Sphingosine and Phytosphingosine Ceramide Ratio on Lipid Arrangement and Barrier Function in Skin Lipid Models. *J. Lipid Res.* **2023**, *64*, 100400. [CrossRef] [PubMed]
40. Zabini, A.; Zimmer, Y.; Medová, M. Beyond Keratinocyte Differentiation: Emerging New Biology of Small Proline-Rich Proteins. *Trends Cell Biol.* **2023**, *33*, 5–8. [CrossRef] [PubMed]
41. Park, I.G.; Jin, S.H.; An, S.; Ki, M.W.; Park, W.S.; Kim, H.J.; Na, Y.; Noh, M. Carnosine and Retinol Synergistically Inhibit UVB-Induced PGE2 Synthesis in Human Keratinocytes through the Up-Regulation of Hyaluronan Synthase 2. *Biomol. Ther.* **2024**, *32*, 635–639. [CrossRef]
42. Treger, D.; Zhang, L.; Jia, X.; Hui, J.H.; Gantumur, M.A.; Hui, M.; Liu, L. A clinical Study of the Local Injection of a Freshly Manufactured 35 kDa Hyaluronan Fragment for Treating Chronic Wounds. *Int. Wound J.* **2024**, *21*, e14906. [CrossRef] [PubMed]
43. Radrezza, S.; Aiello, G.; Baron, G.; Aldini, G.; Carini, M.; D'Amato, A. Integratomics of Human Dermal Fibroblasts Treated with Low Molecular Weight Hyaluronic Acid. *Molecules* **2021**, *26*, 5096. [CrossRef] [PubMed]
44. Radrezza, S.; Baron, G.; Nukala, S.B.; Depta, G.; Aldini, G.; Carini, M.; D'Amato, A. Advanced Quantitative Proteomics to Evaluate Molecular Effects of Low-Molecular-Weight Hyaluronic Acid in Human Dermal Fibroblasts. *J. Pharm. Biomed. Anal.* **2020**, *185*, 113199. [CrossRef] [PubMed]


**Disclaimer/Publisher's Note:** The statements, opinions and data contained in all publications are solely those of the individual author(s) and contributor(s) and not of MDPI and/or the editor(s). MDPI and/or the editor(s) disclaim responsibility for any injury to people or property resulting from any ideas, methods, instructions or products referred to in the content.